The geometry of back arc thrusting along the Eastern Sunda Arc, Indonesia: Constraints from earthquake and gravity data

Article *in* Journal of Geophysical Research Atmospheres · January 1984
DOI: 10.1029/JB089iB07p06171

2 authors:

Rob Mccaffrey
Portland State University
169 PUBLICATIONS **7,153** CITATIONS
SEE PROFILE

John L. Nabelek
Oregon State University
106 PUBLICATIONS **4,699** CITATIONS
SEE PROFILE

JOURNAL OF GEOPHYSICAL RESEARCH, VOL. 92, NO. B1, PAGES 441-460, JANUARY 10, 1987

EARTHQUAKES, GRAVITY, AND THE ORIGIN OF THE BALI BASIN: AN EXAMPLE OF A NASCENT CONTINENTAL FOLD-AND-THRUST BELT

Robert McCaffrey[1] and John Nabelek[2]

Department of Earth, Atmospheric and Planetary Sciences
Massachusetts Institute of Technology, Cambridge

Abstract. We infer from the bathymetry and gravity field and from the source mechanisms and depths of the eight largest earthquakes in the Bali region that the Bali Basin is a downwarp in the crust of the Sunda Shelf produced and maintained by thrusting along the Flores back arc thrust zone. Earthquake source mechanisms and focal depths are inferred from the inversion of long-period P and SH waves for all events and short-period P waves for two of the events. Centroidal depths that give the best fit to the seismograms range from 10 to 18 km, but uncertainties in depth allow a range from 7 to 24 km. The P wave nodal planes that dip south at 13° to 35° (±7°) strike roughly parallel to the volcanic arc and are consistent with thrusting of crust of the Bali Basin beneath it. The positions of the earthquakes with respect to crustal features inferred from seismic and gravity data suggest that the earthquakes occur in the basement along the western end of the Flores thrust zone. The slip direction for the back arc thrust zone inferred from the orientation of the earthquake slip vectors indicates that the thrusting in the Bali Basin is probably part of the overall plate convergence, as it roughly coincides with the convergence direction between the Sunda arc and the Indian Ocean plate. Summation of seismic moments of earthquakes between 1960 and 1985 suggests a minimum rate of convergence across the thrust zone of 4 ±2 mm/a. The presence of back arc thrusting suggests that some coupling between the Indian Ocean plate and the Sunda arc occurs but mechanisms such as continental collision or a shallow subduction of the Indian Ocean plate probably can be ruled out. The present tectonic setting and structure of the Bali Basin is comparable to the early forelands of the Andes or western North America in that a fold-and-thrust belt is forming on the continental side of an arc-trench system at which oceanic lithosphere is being subducted. The Bali Basin is flanked by the Tertiary Java Basin to the west and the oceanic Flores Basin to the east and thus provides an actualistic setting for the development of a fold-and-thrust belt in which structure and timing of deformation can change significantly along strike on the scale a few hundred kilometers.

[1]Also at Air Force Geophysics Laboratory, Hanscom Air Force Base, Massachusetts.

[2]Now at Lamont-Doherty Geological Observatory, Palisades, New York.

Paper number 6B6085.
0148-0227/87/006B-6085$05.00

Introduction

The questions of how and under what conditions fold-and-thrust belts develop in the forelands of continental arcs have been approached largely by studies of well-developed examples such as the Andes and western North America. In both examples, however, the along strike variations in the style of deformation are so great that general cause-and-effect relationships are difficult to infer. Moreover, in only one of the cases (the Andes) can we observe the dip angle of the subducting plate so that inferences about the role of the underthrusting plate in driving the deformation in both examples remain equivocal. Accordingly, studies of other regions where back arc thrusting now occurs are crucial.

One of the clearest examples of present-day back arc thrusting that spans both oceanic and continental settings is the long thrust zone north of the Sunda arc between Java and Wetar [Hamilton, 1979; McCaffrey and Nabelek, 1984, 1986; Silver et al., 1983, 1986; Usna et al., 1979] (Figure 1). The thrust zone is evident in two segments: the Flores thrust zone in the west and the Wetar thrust zone in the east. Both dip opposite to the sense of subduction of the Indian Ocean - Australia plate at the Java Trench and Timor Trough. The Flores thrust zone is the longer and more developed of the two and extends westward, disappearing beneath the Bali Basin [Silver et al., 1983]. Both thrust zones display gravity anomalies, accretionary prisms [Silver et al., 1983], and thrust earthquakes [McCaffrey and Nabelek, 1984, 1986]. So far, no earthquakes that are clearly associated with the back arc thrust zone have been found deeper than 25 km (R. McCaffrey, manuscript in preparation, 1986).

In this paper we focus on the western section of the Flores thrust zone west of Sumbawa and extending into the Bali Basin. Here, the volcanic arc is built on the thick crust of the southern edge of the Asian margin (Sunda Shelf) and thus forms a continental arc, or what is commonly called an "Andean" margin. The Flores thrust zone in this region accommodates the thrusting of the Sunda Shelf in the back arc beneath the volcanic arc and thus is analogous to intracontinental thrust zones such as those today east of the Andes and in western North America in the Cenozoic. In contrast, to the east the Flores and Wetar back arc thrust zones involve oceanic crust of the Flores Basin and Banda Sea. We examine the depths and mechanisms of the eight largest earthquakes from the Bali Basin by inverting their long-period P and SH waves and, in some cases, short-period P waves. In addition, we compile gravity and bathymetry data and present maps for the Bali Basin. We then discuss the

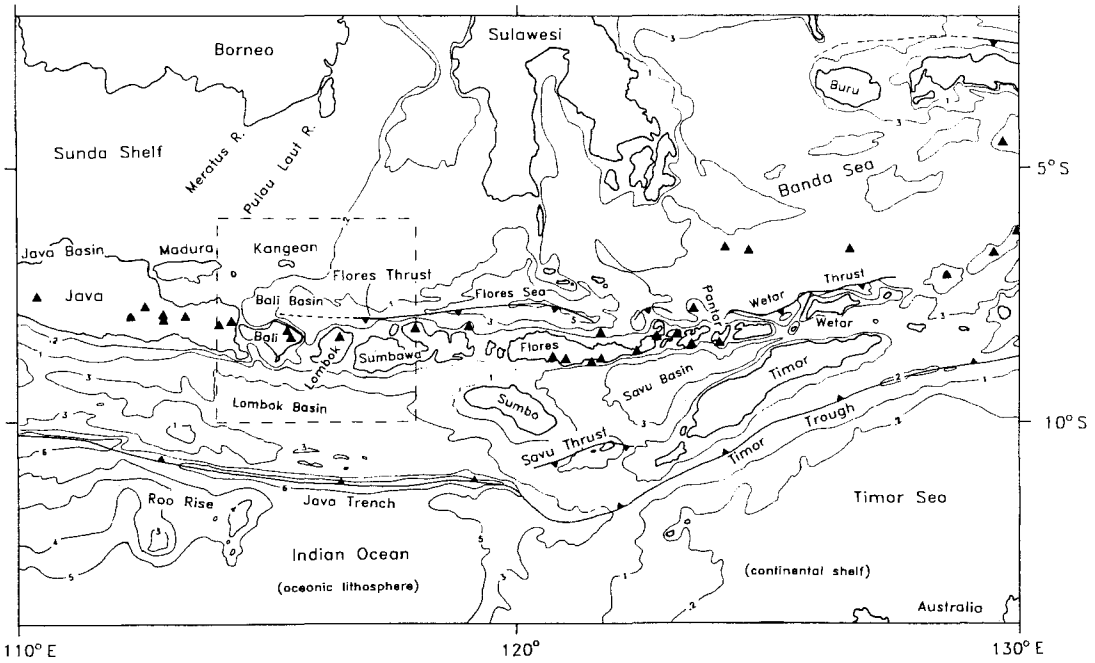

Fig. 1. Tectonic and geographic map of the eastern Sunda arc and vicinity. Active volcanoes are represented by triangles, and bathymetric contours are in kilometers. Thrust faults are shown with teeth on the upper plate. The dashed box encloses the study area.

constraints these data place on the structure and evolution of the Bali Basin and the causes of back arc thrusting, and discuss the implications for the early evolution of fold-and-thrust belts.

The Bali Basin

Setting

The Bali Basin is a narrow, easterly elongated basin in the southeastern part of the Sunda Shelf, with water depth locally exceeding 1.5 km (Figures 1 and 2). Its southern margin is formed by the active volcanic arc. Along strike to the west are the Tertiary Madura and Java sedimentary basins, and to the east is the deeper Flores Sea, likely underlain by oceanic crust [Curray et al., 1977; McCaffrey and Nabelek, 1984].

The southeastern Sunda Shelf is covered by 1 to 2 km, and locally up to 3 km, of sediments and by an average of 200 m of water [Ben-Avraham, 1973; Ben-Avraham and Emery, 1973]. It locally emerges at the islands of Kangean and Madura in an E-W trending ridge. During most of the Pleistocene the portion of the shelf north of Java was a landmass that submerged only recently [van Bemmelen, 1949]. The Java Basin received sediments from both this northern landmass and the volcanic arc to the south [van Bemmelen, 1949; Weeda, 1958]. The eastern Java Basin is now filled with up to 6 km of Tertiary sediments; the lowest 4 km consist of deep water facies, while the upper 2 km show the transition to the present land conditions [Weeda, 1958]. We know of no direct measure of the thickness of sediments in the Bali Basin, but we suggest that there may be approximately 6 km, based on gravity data and the shapes of the seismograms from the earthquakes (discussed below).

Basement rocks of the eastern Sunda Shelf range in ages from 58 to 140 Ma (K-Ar) and consist of terrigenous and volcaniclastic metasediments and volcanic and granitic rocks [Ben-Avraham, 1973; Hamilton, 1979]. The basal sediment layer appears to be of Eocene age. The sedimentary cover is thin or absent over basement ridges that trend either NE (the Pulau Laut and Meratus ridges) or east (the Madura-Kangean Ridge). Ben-Avraham and Emery [1973] note that the sedimentary layers on both sides of the Pulau Laut and Meratus ridges have the same apparent dip as the ridge flanks and do not thicken away from the ridges. This geometry indicates that the ridges formed after deposition of the strata, and the truncation of these ridges and the strata at the seafloor suggest that uplift has ceased. Conversely, the thickening of the sedimentary layers away from the Madura-Kangean Ridge indicates that it has been uplifted during deposition of the sediments, and its present exposure at the two islands suggests that uplift may be continuing. Ben-Avraham and Emery [1973] interpret the Pulau Laut, Meratus, and Madura-Kangean ridges as the roots of anticlines formed by NW-SE and N-S compression.

The islands of Java, Bali, Lombok, and Sumbawa presumably formed by the construction of volcanic arcs on the previously passive southern margin of the Sunda Shelf [Hamilton, 1979]. Along the southern coasts of the islands is a pre-Miocene volcanic arc, while the present volcanoes are situated closer to the northern coasts. Van Bemmelen [1949] noted a NW-SE alignment of volcanic features on Bali and a tendency for younger

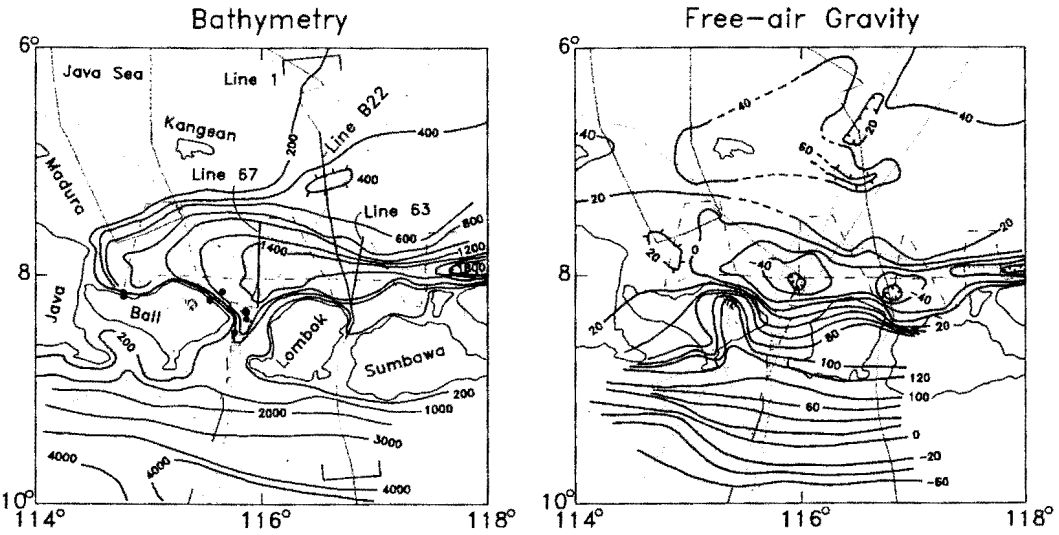

Fig. 2. Bathymetric and free-air gravity maps of the Bali Basin and vicinity. Contours are in meters and mGals (10^{-5} m/s^2), respectively, and are dashed or omitted where control is poor. The lighter points show the locations of measurements. Heavy lines show the locations of lines 63, 67, and B22, and the brackets enclose the data used to construct line 1. Large dots show the locations of the earthquakes discussed in this paper.

eruptions to be more basaltic. Between Flores and Pantar, the volcanic islands are built on oceanic crust, the volcanoes lie along the southern coasts, and the earlier arc is not evident.

Crustal Structure

North of Lombok, the Flores thrust zone has the appearance of a typical oceanic subduction zone in seismic reflection profiles (line 63 in Figure 3). The thick sedimentary section south of kilometer 30 is broadly folded, and the steeper limbs of the asymmetric folds are truncated along predominantly south dipping thrust faults. The increasing dip with depth of planar reflectors beneath kilometer 55 indicates that sedimentation and deformation have occurred concurrently. North of the Flores thrust zone (kilometers 0 to 20) the reflectors seem to arch down into the thrust zone. A comparison with line 67 (Figure 3) shows that the style of deformation changes westward and that the Flores thrust zone loses its surface expression north of Bali. Nevertheless, the broad folding continues and involves the entire sedimentary section, indicating the presence of a decollement surface at depth beneath the sediments [Silver et al., 1983]. The gravity field is not appreciably less negative, indicating that the amount of crustal thickening is similar beneath both lines. Note again the arching of the otherwise undisturbed reflectors from the north into the deeper, southern part of the basin.

Hamilton [1979] suggests that the crust of the Bali Basin was transitional in thickness between oceanic and continental, based on water depth and the assumption that it was in isostatic equilibrium. Ben-Avraham and Emery [1973] infer that

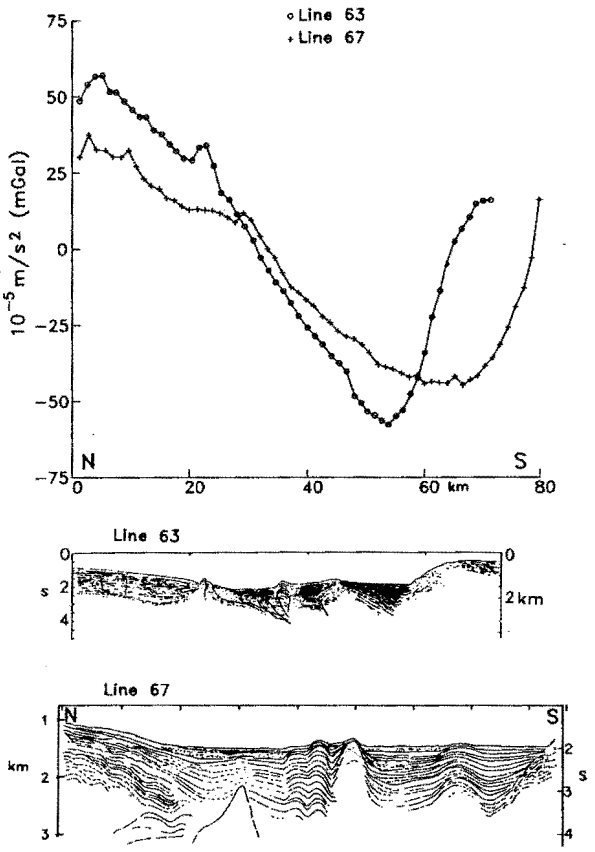

Fig. 3. Free-air gravity profiles and line drawings of seismic reflection profiles [from Silver et al., 1983] across the Bali Basin near Lombok. The locations of these lines are shown in Figure 2.

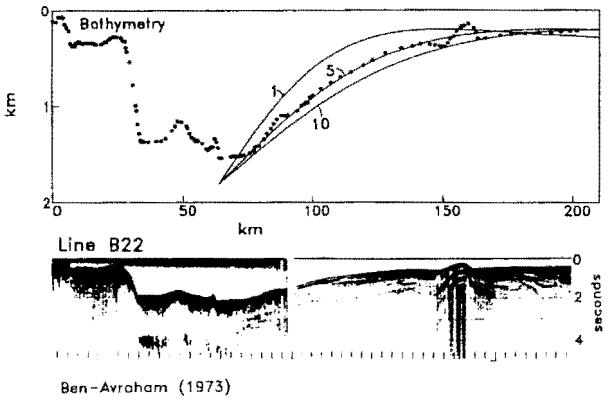

Fig. 4. Seismic profile crossing the southern Sunda Shelf and Bali Basin north of Lombok [from Ben-Avraham, 1973]. Location of profile is shown in Figure 2. The top figure shows the digitized bathymetry (dots) at high vertical exaggeration and theoretical curves for a flexed elastic plate. For a plate deflected vertically at its free end, the solution is of the form $z(x)=z_o \cos(\lambda x)\, e^{-\lambda x}$, where z is the deflection at distance x, z_o is the deflection at x=0, $\lambda=((\rho_m-\rho_w)g/4D)^{1/4}$, g is the gravitational acceleration (9.8 m/s^2), and D is the flexural rigidity of the plate [Watts and Talwani, 1974]. Assumed densities for the mantle and water are ρ_m=3300 kg/m^3, ρ_w=1000 kg/m^3. The curves are for flexural rigidity values of 1, 5, and 10 x10^{22} Nm (as marked).

oceanic crust was present beneath the Bali and Madura basins because of their positions on line with the Flores Basin. Based on the following evidence, we infer that the crystalline crust beneath the Bali Basin is the same thickness as that beneath the Sunda Shelf, and we further surmise that the two are genetically identical. First, the arching of the sediments and of the seafloor from the north into the basin (Figures 3 and 4) indicates that the basin subsided after deposition of the sediments. Continuation of arching into the deepest part of the basin indicates that all of the bathymetric relief can be explained by downbowing of the crust. Second, the minimum in the gravity field over the Bali Basin is displaced 30-40 km south of the minimum in the bathymetry, indicating that isostatic equilibrium does not hold here. More likely, the basement of the Sunda Shelf dips to the south beneath the deformed sediments in the southern Bali Basin, and the deepening of the top of the basement is not accompanied by thinning of the crust. As will be shown, the magnitude of the gravity anomalies is consistent with the idea that the gravity and bathymetric lows are due to downbowing of the crust of the Sunda Shelf. Finally, the bathymetric profile along line 22 of Ben-Avraham [1973] (line B22 in Figure 4) displays the characteristic shape of a flexed lithospheric plate. The estimated flexural rigidity for the Sunda Shelf of 5 to 10 x10^{22} Nm is typical of some oceanic [Caldwell et al., 1976] and continental [Walcott, 1970] regions and corresponds to an effective elastic thickness of 18 to 23 km (Figure 4).

Seismicity

Earthquakes within the Indian Ocean plate define a zone that dips northward from the Java Trench to a depth greater than 600 km beneath the Java Sea (Figure 5). We note, however, that in this region there are few large events that might indicate thrusting of the Indian Ocean plate beneath the fore arc, whereas several normal faulting events have occurred beneath the Java Trench, including the M_S = 8.1 earthquake of August 1977 near 11°S, 118°E. The concentration of hypocenters at 10°S, 117°E is due to shallow strike-slip faulting within the overriding plate during October 1977 [Fitch et al., 1981].

The earthquakes discussed in this paper occurred at shallow depth in the overriding plate beneath the active volcanic arc between Java and Lombok, and several were very destructive. Four caused damage and deaths in the Bali region, including the m_b=6.1 event of July 14, 1976 (our event 3), that reportedly killed 563 people. In the same region, earthquakes in 1815 and 1917 are

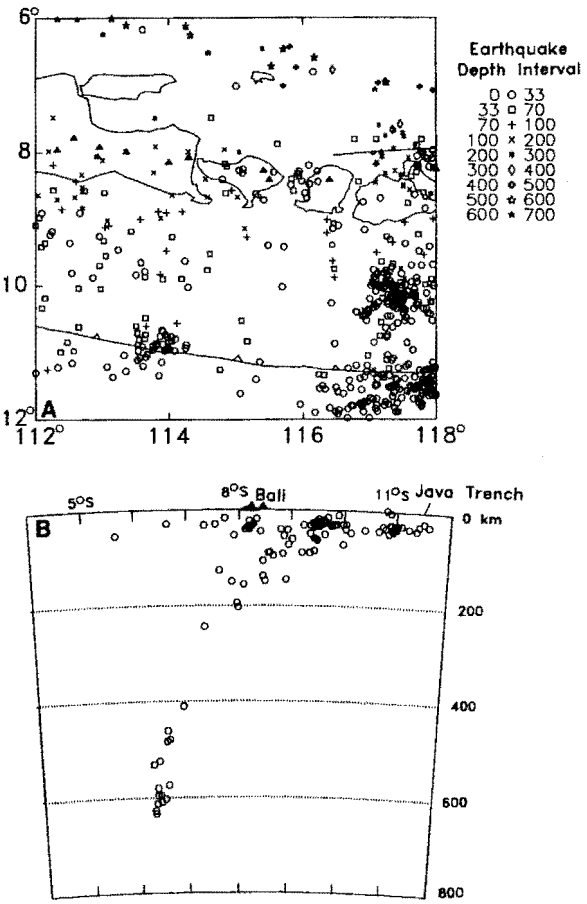

Fig. 5. (a) Seismicity of the Bali region from 1964-1979 (all events listed by the ISC). Depth intervals are in kilometers. (b) Cross section of seismicity in the Bali region. This projection passes through 8°S, 115°E, at an azimuth of 10°, and includes all events within 300 km and recorded by more that 50 seismograph stations. In both plots, triangles show locations of active volcanoes.

TABLE 1. Earthquake Hypocentral and Fault Plane Solution Data

No.	Date	Origin Time[1]	Latitude °S	Longitude °E	Depth, km ISC P	ISC "pP"	Wave-form	Mo[2]	Dura-tion, s	m_b[3]	Auxiliary Plane Strike	Dip	Rake	Fault Plane Strike	Dip	Rake	Phase P	Phase SH	Layer,[4] km W	Layer,[4] km S
1	May 18, 1963	1220:31.5	8.21	115.55	54		16.0±1.0[5]	43 ±25	3.9		259±2	76±2	84±5	102	15	112	13	11	0.0	0
2	May 22, 1963	2153:01.6	8.14	115.66	56		13.4±0.8	79 ±29	2.5		266±2	78±2	83±4	116	14	119	15	14	0.0	0
3	July 14, 1976	713:23.7	8.17	114.79	37	53	13.7±0.6[6]	694 ±84	2.7	6.1	279±2	58±1	87±2	105	32	94	17	7	0.5	6
4	July 14, 1976	1023:46.8	8.15	114.79	41	10	9.6±0.6[7]	42 ±4	1.3	5.9	275±2	58±1	82±2	110	33	102	8	6	0.5	5
5	May 21, 1979	1631:01.8	8.33	115.87	44	36	12.3±1.1	55 ±26	2.9	5.6	265±3	61±2	69±3	123	35	122	7	5	1.3	6
6	May 30, 1979	938:55.3	8.31	115.86	40	20	11.0±0.5	236 ±84	3.4	6.0	271±1	61±1	73±1	123	33	117	19	5	1.5	6
7	Oct. 20, 1979	141:10.3	8.38	115.87	37	38	13.7±0.6	487 ±80	6.0	5.9	270±2	63±1	78±2	115	29	112	20	8	1.5	6
8	Dec. 17, 1979	1958:23.0	8.50	115.76	22	92	18.0±0.8	448±110	5.2	5.6	260±2	75±1	70±4	134	25	141	18	10	1.0	3

[1] Relocated epicenter and origin time in hours, minutes, and seconds.
[2] Seismic moment is in 10^{18} Nm.
[3] Taken from ISC Bulletins.
[4] W represents water depth; S represents sediment thickness.
[5] All quoted formal errors are 2 standard deviations.
[6] 13.3 ±0.2 from short-period data.
[7] 8.0 ±0.3 from short-period data.

reported to have killed 10,253 and 15,000 people, respectively [Ganse and Nelson, 1981].

The ambient level of seismicity in the epicentral regions of the large earthquakes studied here is low. Since all events from the International Seismological Centre (ISC) bulletins are plotted in Figure 5a, note also that very few foreshocks and aftershocks with magnitudes greater than 4.5 to 5.0 were associated with these earthquakes.

Analysis of Earthquakes

Data

The source mechanisms and depths of the earthquakes listed in Table 1 are estimated by matching observed long-period P (vertical component) and SH waves of the World-Wide Standardized Seismograph Network (WWSSN) with synthetic seismograms (Figure 6). Each earthquake is approximated by a point source having a double-couple mechanism. The source parameters are determined by an inversion of the observed data in a least squares sense. The estimated parameters are the strike and dip of one P wave nodal plane, the rake angle on the plane (using the convention of Aki and Richards [1980]), the centroidal (average) depth, seismic moment, and source time function (i.e., source time history). We will refer to each solution by the strike, dip, and rake of its north dipping P wave nodal plane because its strike and dip angles are resolved better than those of the south dipping plane. While the long period data do not contain enough high-frequency information to determine which of the nodal planes is the fault plane, other evidence presented below suggests that it is the south dipping plane. The method used here is described by R. McCaffrey (manuscript in preparation, 1986) and is a modification of that developed by Nabelek [1984, 1985].

Only seismograms recorded at epicentral distances of 30° to 90° for P waves and 30° to 60° for SH waves are used. For the earthquakes presented here, between 12 and 29 seismograms are included in the inversion (Table 1). Data are the amplitudes of the observed seismograms, digitized at 0.25-s intervals, within a specified time window starting at the direct phase (P or S) and extending through the reflected (pP, sP, and sS) and other converted phases. A causal attenuation operator [Futterman, 1962] is applied with a ratio of travel time to average Q of 1s for P waves, and of 4s for SH waves. The source region crustal structure assumed in generating the seismograms consists of a water layer, sediment layer (v_p=3.2 km/s, v_s=1.8 km/s, density ρ=2300 kg/m^3), over a half space (v_p=6.5 km/s, v_s=3.7 km/s, ρ=2800 kg/m^3). The P wave velocities are based on seismic refraction results reported by Ben-Avraham and Emery [1973], Curray et al. [1977], and Raitt [1967]. The thicknesses of the water and sediment layer (Table 1) are adjusted to match specific characteristics of the waveforms. The response of the source structure is calculated by summing a finite number of rays (R. McCaffrey, manuscript in preparation, 1986). Structure at each receiver is assumed to be a half space (v_p=6.0 km/s, v_s=3.4 km/s, ρ=2700 kg/m^3).

24 km (appendix). These depths are generally much shallower than those reported by the ISC, including those based on "pP" readings (Table 1), and further indicate the unreliability of the ISC depths for this region [R. McCaffrey, manuscript in preparation, 1986]. The new source depths are unequivocal evidence that these earthquakes are related to deformation of the overriding plate and not to interplate or slab activity.

Stress Drops

A striking feature of the westernmost events (3 and 4) is that their source time functions are short when compared with any of the other events of similar seismic moment and that the moment of event 3 is 10 times larger than that of event 5, which has a similar duration (Table 1). In a (single asperity) circular crack model, the stress drop is proportional to M_o/t^3 [e.g., Boatwright, 1980], where t is the source duration (Table 1). Because M_o/t^3 is roughly an order of magnitude higher for events 3 and 4 than for the others, it is likely that these two events had a much higher stress drop. It is unlikely that the difference is due to error, as this would require a factor of 2 error in duration or a factor of 10 error in moment.

The higher stress drop for events 3 and 4 relative to those of the eastern events denotes some change in the properties of the fault zone. The geometry of the Flores thrust zone suggests that the amount of slip that has already occurred decreases westward. Accordingly, events 3 and 4 may have occurred in crust that is less fractured and thus stronger than that to the east. The 1978 Flores and 1977 Timor earthquakes that occurred on the more developed part of the Flores thrust zone and on the Wetar thrust zone, respectively, are also of the low stress drop type [McCaffrey and Nabelek, 1984, 1986].

Estimate of the Minimum Slip Rate

To calculate the minimum slip rate for the Bali Basin, we use the relation $\Sigma u = \Sigma M_o/\mu A$ normalized by the time period [Brune, 1968]; u is the average slip for one event, the rigidity $\mu = \rho v_s^2$ (3.8×10^{10} N/m^2), and A is the area of the fault surface on which the earthquakes occurred. The total moment ΣM_o released by the eight earthquakes is $2 \pm 1 \times 10^{19}$ Nm (the uncertainty of 50% is based on the analysis in the appendix). The fault length along strike is estimated at 150 km (Figure 7a) and its downdip length at 40 km (Figure 7b), for an area of 6×10^9 m^2. The time period is 25 years (1960-1985). From the relation above, the total slip is 0.09 ±0.04 m, and the slip rate is 4 ±2 mm/a (rounded to the nearest mm/a). By a global fit of the plates, the expected convergence rate between the Indian Ocean and Asian plates near Bali is approximately 70 mm/a [Minster and Jordan, 1978]; thus the rate of slip across the Flores thrust zone in the Bali Basin, estimated from seismic energy release, is minor compared with the expected convergence rate between the major plates. We emphasize, however, that the lack of large thrust earthquakes beneath the Sunda fore arc [Kelleher and McCann, 1976] indicates that the seismic slip rate here is also low compared with the plate motion rate. The concentration of thrust earthquakes along the southern margin of the back arc basin is characteristic of the Banda arc also [McCaffrey and Nabelek, 1986].

Earthquake Locations

The eight earthquakes are relocated using the P tables of Herrin [1968], P wave arrival times from ISC Bulletins, and the depths determined from the waveform analysis (Table 1). The relocated epicenters are shifted northward by about 5 km relative to the locations determined by the ISC but retain their original pattern of grouping.

Other evidence supports the relative locations determined with arrival time data and gives some insight into the absolute locations of the events. Event 3 produced much damage in western Bali and was felt on Java. Its location beneath the island is suggested by a microearthquake study (D. Z. Hayat and S. Panjaitan, unpublished report, 1983) in which shallow seismic activity beneath western Bali was recorded; however, the level of activity offshore could not be monitored. The sequence of events 5 - 8 seems to have migrated from the vicinity of Lombok toward Bali. Events 5 and 6 caused major damage on Lombok but little damage on Bali. Event 7 caused considerable damage on both islands, whereas the damage caused by event 8 was concentrated on Bali. Event 8 produced maximum Modified Mercalli intensity of IX east of Gunung Agung (the southern volcano on Bali) at Culik (8.3°S, 115.6°E) [Effendi et al., 1981], suggesting a nearby epicenter. This constraint on the epicenter of event 8 suggests that the epicentral positions shown in Figure 7 should be shifted approximately 10 km northward. A microearthquake study southeast of Gunung Agung (M. B. Wismaya, unpublished report, 1981) also revealed shallow seismic activity beneath Bali Island. Finally, the requirement of a thick sediment layer in the source structure to match the waveforms coupled with the constraints on structure from the gravity data discussed below, suggests that the earthquakes were farther north, beneath the basin, where sediments are more likely to be the requisite thickness.

The alignment of the relocated hypocenters in a projection onto a vertical plane that is roughly parallel to the slip direction (Figure 7b) suggests that the south dipping plane is the fault plane. Because of uncertainties in both the epicenters and depths, and in the appropriate projection, this independent determination of the fault plane from the earthquake positions alone must be considered inconclusive. Nevertheless, the sense of displacement on the Flores thrust zone inferred from seismic reflection profiles and gravity data suggests a south dipping plane, and the fault plane solutions indicate that this plane dips between 10° and 30°. No significant change in dip angle with depth is apparent.

Gravity Interpretation

Data

The gravity map (Figure 2) and line 1 (Figure 10a) are constructed from gravity data

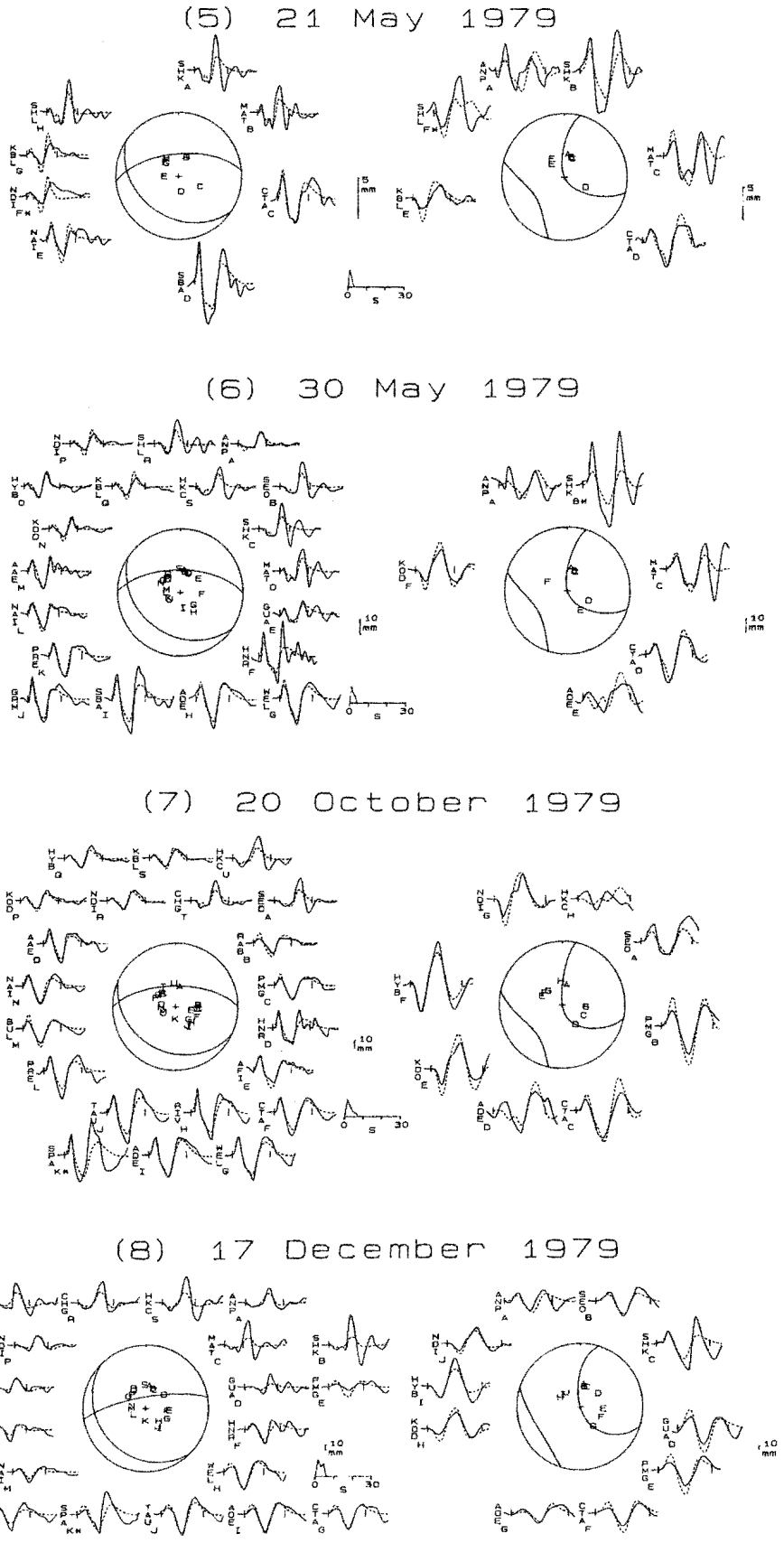

Fig. 6 (continued)

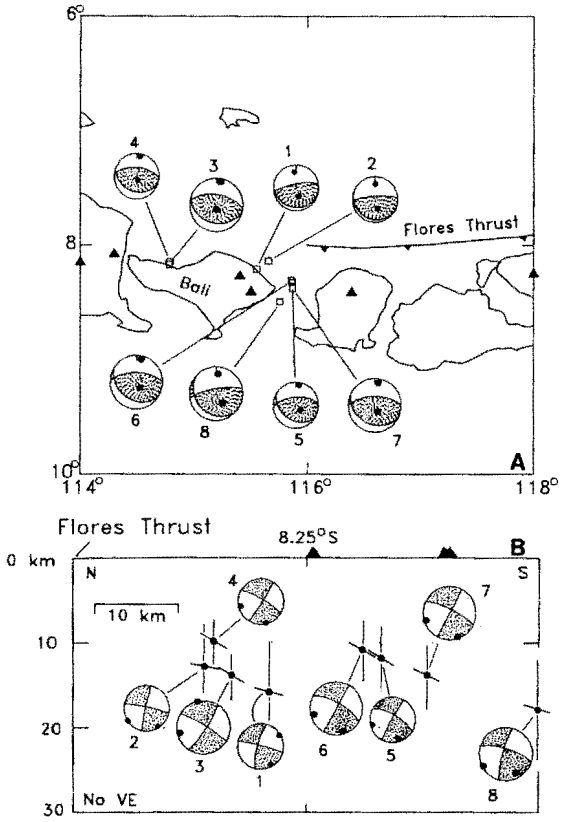

Fig. 7. (a) Lower hemisphere projections of fault plane solutions near Bali Island determined in this study. Stippled quadrants are those with compressional P wave first motions. P and T axes are shown by large dots. Events shown with larger focal spheres have seismic moments greater than 10^{18} Nm. (b) Cross section of Bali earthquakes with side projections of their fault plane solutions. The dipping lines through the hypocenters represent the projections of the inferred fault planes, and the vertical lines show the range of possible depths.

Fault Plane Solutions

The best fitting fault plane solutions and the observed and calculated seismograms are shown in Figure 6. The solutions are also plotted in both map and cross-sectional views in Figure 7. The uncertainties in the source parameters given in Table 1 are the statistical uncertainties and underestimate the true uncertainties. An evaluation of the actual uncertainties for individual events is presented in the appendix, and the general results are depth ±5 km, seismic moment ±50%, strike ±20°, dip ±5°, and rake ±20°.

Events 1 and 2 occurred near the NE coast of Bali in 1963. Event 1 caused more damage on Bali although it was deeper and smaller in seismic moment than event 2. These differences imply that event 1 was located beneath the island while event 2 was offshore (Figure 7). The north dipping nodal plane of event 2 is constrained by stations AAE, SHI, and QUE in the west and GUA in the east. The similarity of the seismograms (especially from QUE that lies very close to the nodal plane) for the two events suggests that they had similar mechanisms. Of the events studied here, these have the shallowest south dipping nodal planes (15° and 14°).

Events 3 and 4 occurred near the north-central coast of Bali and were separated from the other six. Again, the north dipping nodal plane for event 3 is constrained by the northern stations; note the change in the initial P pulse in proceeding azimuthally from CHG (up) to HKC and ANP (nodal) to SHK and MAT (up). The depths of these two events estimated from the short-period P seismograms (Table 1 and Figure 8) agree to within 2 km with the depth obtained from long-period data. This agreement is compelling evidence that the long-period waveforms do have sufficient information to constrain the depths of these earthquakes to within a few kilometers.

Events 5, 6, 7, and 8 occurred in 1979 beneath the strait separating Bali and Lombok islands. All four were damaging, and events 6, 7, and 8 caused fatalities. Note the strong similarity of waveforms among the events with the significant exception of the initial half cycle at stations in the vicinity of the north dipping nodal plane.

For many of the events, long-period seismograms at stations near the north dipping P wave nodal plane display a sharp initial pulse and a W-shaped trough (for example, see NDI, CHG, SHK, and MAT for event 3; Figures 6 and 9). This shape is caused by the presence of two phases with negative polarity (consistent with the expected polarity of pP; sP is expected to be positive) and a few seconds separation; the first causes the sharp turnaround of the P, and the second produces the second trough of the W. Note in Figure 9 that both the long-period and short-period records at HKC are nodal (the correlation of later phases between HKC and SHK shows that HKC has no direct P wave) and that the first pulse observed is the first of these negative polarity phases. The wave shape at the northern stations cannot be explained by adjusting the source depth, the source time function (Figures 9a and 9b), or the thickness of the water layer within limits found in the epicentral region (Figure 9c). A typical Moho interface cannot produce the observed amplitudes.

In order to match this feature of the observed waveforms, in addition to a water layer, a thick layer with low seismic velocities comparable to those of sediments is required in the source region (Figures 9d, 9e, and 9f). In this case, the first negative pulse is a p wave reflection from the bottom of the sediment layer, while the second is a combination of the p wave reflections from the tops of the sediment and the water layer. The thickness of the sediment layer must be such that it produces the time difference between the phases, while the impedance contrast at its base must be large enough to produce the observed amplitudes. The comparison of the synthetic seismograms produced for a range of structures (with their best fitting solutions) indicates that about 6 km of sediments are required by both the long- and short-period P waves (Figure 9). This thickness of sediments is probably only found beneath the Bali Basin and not beneath Bali Island or Lombok Strait, where the earthquakes are located using P wave arrival times. Thus it is likely that the earthquakes occurred more to the north than their computed

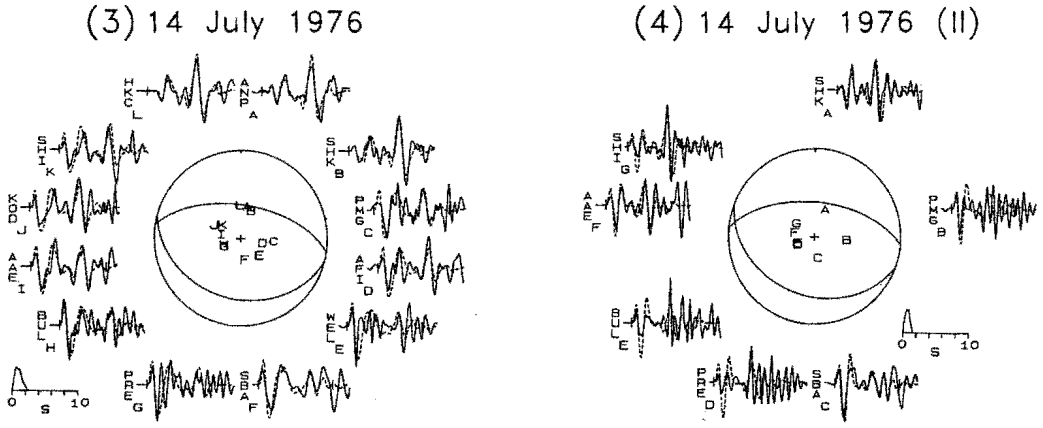

Fig. 8. Short-period P wave seismograms for events 3 and 4. The fault plane solutions and source structures are the same as for the long-period data (Figure 6 and Table 1). Amplitudes have been normalized by the rms amplitude within the inversion window.

locations indicate. Similar mislocations are inferred for the 1978 earthquake on the Flores thrust zone based on waveform data [McCaffrey and Nabelek, 1984] and for several large events near Timor based on locally recorded arrival time data [McCaffrey et al., 1985].

Fault plane solutions for events 1-4 were determined from P and S wave first-motion polarity readings in previous studies (event 2 by Fitch [1970] and events 1, 3, and 4 by Kappel [1980]). The best fitting strike angles of all new solutions fall within 10° of 269° (possibly indicating a smaller uncertainty in strike than the 20° estimated in the appendix), whereas those of the earlier solutions ranged from 276° to 290°. All earlier solutions are characterized by rake angles of 90° (i.e., pure thrust), whereas the revised solutions indicate a systematic deviation from pure thrust (all best fit rake angles are within 9° of 78°). The horizontal projections of the slip vectors (i.e., normal to the strike of the auxiliary plane) are all within 10° of N. The convergence direction in the Bali Basin indicated by the slip vectors is essentially identical to the Indian Ocean - Eurasia convergence direction determined by Cardwell et al. [1981] (0°) and is similar to that predicted by Minster and Jordan [1978] (20°).

Centroid Depths

The best fitting centroid depths determined by the waveform analyses range from 10 to 18 km, but the uncertainties in depths allow a range of 7 to

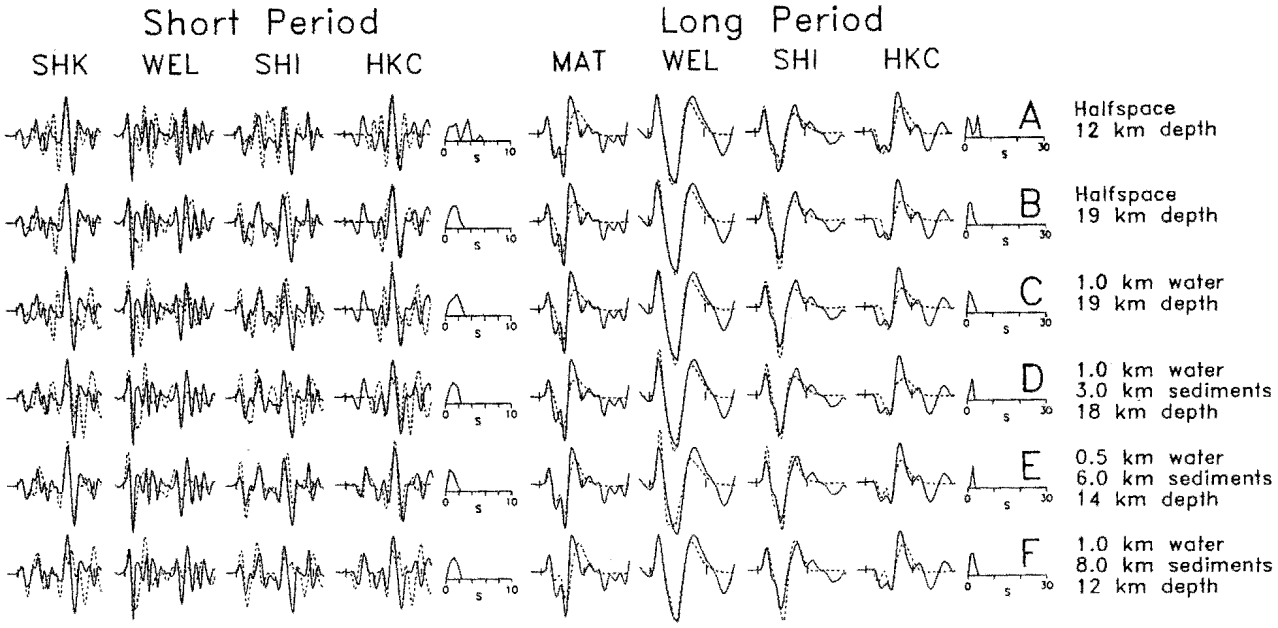

Fig. 9. Selected short- and long-period P seismograms for event 3, used to examine the effects of the assumed source structure on the waveforms. For the short-period data, the amplitudes are normalized (see Figure 8) and the source orientation is fixed. The orientation was allowed to vary for the long-period data. Clearly, the best fit to both the long- and short-period data is for case E.

24 km (appendix). These depths are generally much shallower than those reported by the ISC, including those based on "pP" readings (Table 1), and further indicate the unreliability of the ISC depths for this region [R. McCaffrey, manuscript in preparation, 1986]. The new source depths are unequivocal evidence that these earthquakes are related to deformation of the overriding plate and not to interplate or slab activity.

Stress Drops

A striking feature of the westernmost events (3 and 4) is that their source time functions are short when compared with any of the other events of similar seismic moment and that the moment of event 3 is 10 times larger than that of event 5, which has a similar duration (Table 1). In a (single asperity) circular crack model, the stress drop is proportional to M_o/t^3 [e.g., Boatwright, 1980], where t is the source duration (Table 1). Because M_o/t^3 is roughly an order of magnitude higher for events 3 and 4 than for the others, it is likely that these two events had a much higher stress drop. It is unlikely that the difference is due to error, as this would require a factor of 2 error in duration or a factor of 10 error in moment.

The higher stress drop for events 3 and 4 relative to those of the eastern events denotes some change in the properties of the fault zone. The geometry of the Flores thrust zone suggests that the amount of slip that has already occurred decreases westward. Accordingly, events 3 and 4 may have occurred in crust that is less fractured and thus stronger than that to the east. The 1978 Flores and 1977 Timor earthquakes that occurred on the more developed part of the Flores thrust zone and on the Wetar thrust zone, respectively, are also of the low stress drop type [McCaffrey and Nabelek, 1984, 1986].

Estimate of the Minimum Slip Rate

To calculate the minimum slip rate for the Bali Basin, we use the relation $\Sigma u = \Sigma M_o/\mu A$ normalized by the time period [Brune, 1968]; u is the average slip for one event, the rigidity $\mu = \rho v_s^2$ (3.8×10^{10} N/m^2), and A is the area of the fault surface on which the earthquakes occurred. The total moment ΣM_o released by the eight earthquakes is $2 \pm 1 \times 10^{19}$ Nm (the uncertainty of 50% is based on the analysis in the appendix). The fault length along strike is estimated at 150 km (Figure 7a) and its downdip length at 40 km (Figure 7b), for an area of 6×10^9 m^2. The time period is 25 years (1960-1985). From the relation above, the total slip is 0.09 ± 0.04 m, and the slip rate is 4 ± 2 mm/a (rounded to the nearest mm/a). By a global fit of the plates, the expected convergence rate between the Indian Ocean and Asian plates near Bali is approximately 70 mm/a [Minster and Jordan, 1978]; thus the rate of slip across the Flores thrust zone in the Bali Basin, estimated from seismic energy release, is minor compared with the expected convergence rate between the major plates. We emphasize, however, that the lack of large thrust earthquakes beneath the Sunda fore arc [Kelleher and McCann, 1976] indicates that the seismic slip rate here is also low compared with the plate motion rate. The concentration of thrust earthquakes along the southern margin of the back arc basin is characteristic of the Banda arc also [McCaffrey and Nabelek, 1986].

Earthquake Locations

The eight earthquakes are relocated using the P tables of Herrin [1968], P wave arrival times from ISC Bulletins, and the depths determined from the waveform analysis (Table 1). The relocated epicenters are shifted northward by about 5 km relative to the locations determined by the ISC but retain their original pattern of grouping.

Other evidence supports the relative locations determined with arrival time data and gives some insight into the absolute locations of the events. Event 3 produced much damage in western Bali and was felt on Java. Its location beneath the island is suggested by a microearthquake study (D. Z. Hayat and S. Panjaitan, unpublished report, 1983) in which shallow seismic activity beneath western Bali was recorded; however, the level of activity offshore could not be monitored. The sequence of events 5 - 8 seems to have migrated from the vicinity of Lombok toward Bali. Events 5 and 6 caused major damage on Lombok but little damage on Bali. Event 7 caused considerable damage on both islands, whereas the damage caused by event 8 was concentrated on Bali. Event 8 produced maximum Modified Mercalli intensity of IX east of Gunung Agung (the southern volcano on Bali) at Culik (8.3°S, 115.6°E) [Effendi et al., 1981], suggesting a nearby epicenter. This constraint on the epicenter of event 8 suggests that the epicentral positions shown in Figure 7 should be shifted approximately 10 km northward. A microearthquake study southeast of Gunung Agung (M. B. Wismaya, unpublished report, 1981) also revealed shallow seismic activity beneath Bali Island. Finally, the requirement of a thick sediment layer in the source structure to match the waveforms coupled with the constraints on structure from the gravity data discussed below, suggests that the earthquakes were farther north, beneath the basin, where sediments are more likely to be the requisite thickness.

The alignment of the relocated hypocenters in a projection onto a vertical plane that is roughly parallel to the slip direction (Figure 7b) suggests that the south dipping plane is the fault plane. Because of uncertainties in both the epicenters and depths, and in the appropriate projection, this independent determination of the fault plane from the earthquake positions alone must be considered inconclusive. Nevertheless, the sense of displacement on the Flores thrust zone inferred from seismic reflection profiles and gravity data suggests a south dipping plane, and the fault plane solutions indicate that this plane dips between 10° and 30°. No significant change in dip angle with depth is apparent.

Gravity Interpretation

Data

The gravity map (Figure 2) and line 1 (Figure 10a) are constructed from gravity data

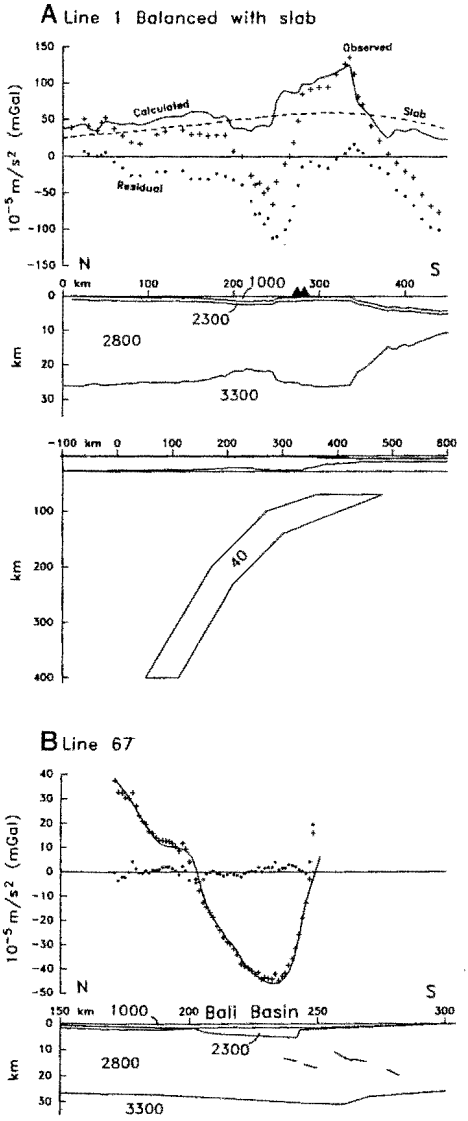

Fig. 10. Structural models and gravity data for the Bali Basin. The numbers in each layer give its density in kg/m³ (except for the slab in which the density contrast is given). (a) Isostatically balanced model along line 1. The top diagram shows crustal structure (vertical exaggeration of 4), and the bottom shows the entire assumed structure (no vertical exaggeration). (b) Structural model beneath line 67 that satisfies gravity data and assumes a constant thickness for the crystalline crust of the Sunda Shelf. The small lines beneath kilometers 250 to 280 show the relocated positions of the earthquakes (based on arrival time data) relative to this model. The slopes of the lines show roughly the dips of the inferred fault planes for the events. Note that the waveform data suggest that some of the earthquakes occurred beneath thick sediments that are probably found 10 to 30 km to the north of the positions shown.

compiled by C.O. Bowin [see Bowin et al., 1982] and the gravity data from the RAMA 12 cruise in 1981 [Silver et al., 1983]. All gravity measurements are reduced to their free-air anomalies with respect to the Geodetic Reference System 67 formula [e.g., Woollard, 1979]. The gravity values on Bali Island are reduced to simple Bouguer anomalies using the infinite sheet approximation and a density of 2700 kg/m³. Gravity and bathymetry values are averaged over 5x5 km areas and contoured at 20-mGal (2×10^{-4} m/s²) intervals (Figure 2).

In order to obtain the long profile (line 1) over the Sunda Shelf, Bali Basin, and the Sunda island arc, all gravity and bathymetry measurements within 30 km of a line passing southward through 6°S, 116.41°E at an azimuth of 175° are averaged at 5-km spacings. The gravity anomalies along lines 63 and 67 (Figure 3) are taken from the RAMA 12 data but are not averaged. In the following figures, all profiles are referenced to the same x axis with x=0 at 6°S.

Gravity Map (Figure 2)

The Bali Basin is associated with a low in the free-air gravity field that follows the northern coasts of the volcanic islands. The low reaches below -60 mGal north of the straits between Bali and Lombok and between Lombok and Sumbawa. The low is truncated at 115°E by a high north of western Bali. Over the Madura-Kangean Ridge there is a gravity high of 40 to 60 mGal that is likely caused by the combination of a regional high and the proximity of higher density basement rocks to the seafloor [Ben-Avraham and Emery, 1973].

The latitudinal widths of both the gravity and bathymetric lows associated with the back arc thrust zone appear to increase westward from Sumbawa (Figures 2 and 3). We note that throughout the length of the Flores thrust zone, such variations in width are common [Silver et al., 1983], but to the east the regions of greater width are usually associated with more thrusting and folding than the narrower sections. Beneath the Bali Basin, however, the zone of deformation is wide, but the amount of shortening in the sediments appears to be small. The broadening of the deformed zone probably signals a change in mechanical behavior, most likely in the sediments, once the thrust zone steps onto the Sunda Shelf.

Isostatically Balanced Model of Line 1

Gravity and bathymetric data show a strong negative in the gravity field over the deep parts of the Bali Basin and then an increase in gravity over the island arc. In order to determine whether or not the crustal structure is in isostatic equilibrium, we generate an isostatically balanced model (including the estimated effect of the subducted Indian Ocean plate) for line 1 and compare the calculated gravity with that observed. The difference in gravity (the isostatic anomaly) is an indication of the amount of noncompensation for topographic features. The isostatically balanced crustal model and its gravity effect are shown in Figure 10a.

To generate the balanced model, we assume that the Sunda Shelf is in isostatic equilibrium. This is a safe assumption, since enormous stresses would be required to keep such a great area out of equilibrium. For the shelf, we assume a crustal thickness of 25 km (ρ_c=2800 kg/m³). The

average water depth of 0.1 km (ρ_w=1000 kg/m^3) and sediment thickness of 1 km (ρ_s=2300 kg/m^3) are then balanced by a mantle layer thickness of 1.9 km (ρ_m=3300 kg/m^3) using the relation $h_w(\rho_w-\rho_o) + h_s(\rho_s-\rho_o) + h_m(\rho_m-\rho_o) = 0$, where h is the thickness of the layer whose initial is in the subscript. The depth of compensation (H) is 28 km, and the average density (ρ_o) is 2800 kg/m^3. To compensate for the changes in water depth, the crustal thickness h_c is varied locally using the relation above, and the relation $h_c=H-h_w-h_s-h_m$. The sedimentary layer is included in order to employ a correct density for many of the bathymetric features, but because its thickness is kept constant, it has a negligible effect on the long-wavelength part of the computed anomaly.

In addition, we include the subducted slab of the Indian Ocean plate (Figure 10a) to account for the regional gravity high over the Sunda Shelf [Ben-Avraham, 1973]. The position and shape of the slab are based on earthquake locations (Figure 5). A density contrast with respect to the mantle of 40 kg/m^3 is chosen to match roughly the amplitude of the field over the Sunda Shelf and to be consistent with the observable gravity effect of slabs in other parts of the world [Grow and Bowin, 1975; Molnar, 1977; Watts and Talwani, 1975]. The gravity effect of the assumed slab structure (shown by a dashed line in Figure 10a) is +35 mGal over the northern end of the profile and increases to a maximum of +70 mGal over the island arc. Note that the inclusion of the slab as shown also implies isostatic equilibrium for the volcanic islands; they would otherwise have a strongly negative isostatic anomaly.

The residual gravity of ≃ -100 mGal for the isostatically balanced model (isostatic anomaly) indicates that the low free-air anomaly observed over the Bali Basin is not an effect of the juxtaposition of crustal elements of different thicknesses (i.e., an edge effect). We conclude that the crust beneath the Bali Basin does not thin to accommodate the increase in water depth; instead it appears to be deflected downward, and the void is filled by water and sediments.

Crustal Structure Beneath Line 67

In order to estimate how much the crust beneath the Bali Basin is downwarped, an isostatically balanced, constant crustal thickness model of the Sunda Shelf is perturbed by varying the thickness of the sediment layer until agreement with the gravity data is obtained (Figure 10b). The gravity profile for line 67 (Figure 3b) rather than line 1 is used because this line is closer to where the thrust earthquakes occurred. Again the densities and thicknesses noted above for the isostatically balanced Sunda Shelf are assumed for this profile and the slab structure is included.

To match the gravity data the following perturbations are necessary (Figure 10b): (1) thickening the sedimentary layer to 4 km beneath kilometer 240, (2) a sharp offset in basement at kilometer 240, (3) a small ridge in basement beneath kilometer 200, and (4) thinning the sediment layer beneath the southern end of the line. Thickening of the sediments beneath the Bali Basin is necessary to produce the large gravity negative. While the amount of sediment thickening depends on the assumed densities, the important point is that thickening by downbowing of the crust is required. If the crystalline crust was thinner beneath the basin, then even more downbowing is indicated. For the densities used here the dip angle of the basement between kilometers 210 and 240 is about 3°. The dip angle of the major thrust surface of the Flores thrust zone between kilometers 20 and 35 in Figure 3a is slightly larger, 6°, probably because, as can be seen in Figure 3a, the thrust plane splays from a probable decollement surface at depth up through the sedimentary section.

The sharp crustal offset at kilometer 240 and the thinning of the sediments south of that point are demanded by the sharp gradient in gravity from kilometers 240 to 250. Even with a vertical offset in basement, the calculated gradient is less than that observed. While the observed gradient may indicate a greater density contrast between the crust and sediments, the lack of correlation between the gravity field and bathymetry in the strait between Bali and Lombok (Figure 2) suggests that it is more likely due to structures to the sides of the profile. Note that the contour lines of bathymetry are nearly tangential to the profile line at its southern end (Figure 2) and thus the assumption of structural two-dimensionality is violated. Finally, since the crustal thickness is kept constant, deflection of the Moho is implied, but we point out that the gravity data are insensitive to such details of the shape of the Moho.

Discussion

Causes of Thrusting

In the section of the Sunda arc from Java to Wetar, the convergent margin changes from one of subduction of old oceanic crust (Indian Ocean) beneath a continental margin (Sunda Shelf) in the west, to one of subduction of continental crust (Australia) beneath an island arc built on oceanic crust (Banda arc) in the east. In the east, most of the deformation of the island arc can be attributed to collision with the Australian continent. In the Flores section, the deformation of the arc is probably caused by interaction between the subducting Australian margin and a thick crustal block (Sumba) within the fore arc. At the western end, near Bali, however, there is no obvious local cause of the thrusting north of the volcanic arc.

One explanation for the presence of thrusting in the Bali Basin offered by Silver et al. [1983] is lateral propagation of the Flores thrust zone from the east. This mechanism requires that the arc structure act as a beam when it is indented. Because the arc itself is cut extensively by strike-slip faults and because the northward displacement of the volcanic islands north of Timor and Sumba appears to occur only locally, we feel that lateral propagation of the back arc thrusting is inefficient and does not offer a viable explanation.

Hamilton [1979] suggests a mechanism for the thrusting that calls on the intrusion of magmatic material and requires no external forces or net shortening across the arc. He observes that on

Java "compressional structures in Neogene materials tend to arc concentrically around, and to be directed outward from, large volcanic edifices." He suggests that the downbowing that allowed the formation of sedimentary basins was due to loading of the crust by volcanoes and that subsequent deformation of the sediments was caused "partly by gravitational flow of the upper crust and its sedimentary cover in response to magmatic loading, and partly by spreading of the crust in the magmatic belt by intrusions within it."

The distinction between the mechanism advocated by Hamilton in which no net shortening across the volcanic arc structure occurs and one in which shortening does occur is basic to our understanding of island arcs, collisions, and whether or not island arcs can reverse subduction direction. While other circumstances may apply to arcs in general, we favor the presence of shortening across the Sunda island arc based on our studies here. First, the lower crustal depths and shallowly dipping nodal planes for the earthquakes beneath the Bali Basin are evidence that basement is actively involved in the thrust faulting. Second, the similarity of the fault plane solutions despite the different locations of the earthquakes relative to the active volcanoes suggests that the direction of thrusting is not controlled by the positions of the volcanoes. This observation is more consistent with uniform slip of the island arc over the back arc basin. Finally, the most critical evidence is the locations of these earthquakes and their relationship to the volcanoes on Bali and Lombok islands. The locations based on arrival time data (Figure 7) and the intensity reports suggest that the thrust earthquakes and thus the thrust fault zone extend beneath the active volcanoes. If so, then mechanisms for the thrusting that rely on swelling of the arc by magmatic intrusion from beneath cannot apply, and regional compression of the volcanic arc must be invoked. Silver et al. [1983] also reject the magmatic intrusion mechanism because the back arc thrusting is observed where there are no volcanoes and because of the absence of obvious extensional features within the arc in places where back arc thrusting is well developed and significant slip (i.e., tens of kilometers) has occurred (e.g., Flores). The absence of N-S extension is also indicated by fault plane solutions for shallow earthquakes within the arc and fore arc; these are predominantly strike slip and indicate N-S shortening (R. McCaffrey, manuscript in preparation, 1986).

What causes the N-S compression across the arc? The convergence directions between the Sunda Shelf and the island arc in the Bali Basin indicated by slip vectors and between the Indian Ocean plate and Asia [Cardwell et al., 1981; Minster and Jordan, 1978] are nearly parallel suggesting that plate motions are driving the back arc thrusting, probably through coupling of the plates beneath the fore arc. Such coupling could be produced by shallow subduction of the Indian Ocean plate, but we cannot document this because the uncertainties in the earthquake hypocenters do not permit adequate resolution of the subduction angle of the Indian Ocean plate at shallow depths beneath the fore arc south of Bali and Lombok. There are some indications, however, that subduction may be steep here. The subducting oceanic crust is very old; both magnetic anomaly lineations [Larson, 1975] and the presence of upper Jurassic basal sediments in Deep Sea Drilling Project hole 261 (at 13°S, 118°E) indicate an age of about Late Jurassic to Early Cretaceous. The Lombok Basin is the deepest section of the fore arc basin (with the exception of the Weber Deep far to the east), and the Java Trench appears to be slightly deeper south of the Lombok Basin (Figure 1). There have been no large thrust earthquakes here [Kelleher and McCann, 1976], but there have been several normal faulting events at the trench (possibly related to sharp downbending of the oceanic plate) [Cardwell and Isacks, 1978], including the M_S=8.1 Sumba earthquake of 1977. The foregoing observations might argue for a steep subduction angle and very weakly coupled subduction. In fact, considerations of such factors as slab dip (at greater depths beneath the arc), convergence rate, lithospheric age, and maximum earthquake size place the Java Trench globally among subduction zones at which back arc spreading, and not back arc compression, occurs [Ruff and Kanamori, 1980; Uyeda and Kanamori, 1979].

Alternatively, as Silver et al. [1983] suggest, and we favor this view, the thrusting in the Bali Basin may be due to collision with the Roo Rise, a bathymetric high that intersects the Java Trench between 110° and 115°E (Figure 1) and probably extends to the NE beneath the fore arc south of Bali. Kelleher and McCann [1976] infer that the Roo Rise resists subduction because of its buoyancy and is responsible for the lack of great thrust earthquakes in the fore arc south of Java. Details of the interaction of the Roo Rise with the fore arc are lacking, but lateral changes in fore arc structure appear to coincide with the Roo Rise (the fore arc outer ridge is more elevated and the fore arc basin is narrower here than to the east, and the Java Trench appears to be slightly indented [Hamilton, 1979]), indicating that some modification of the subduction process is taking place.

Analogy With the Andes and Western North America

In the forelands of both the Andes and western North America, two styles of deformation are dominant; (1) the thin-skinned style of the Canadian Rockies [Bally et al., 1966; Price, 1981; Price and Mountjoy, 1970], Sevier Desert [Armstrong, 1968], Bolivia, and Argentina [Jordan et al., 1983] and (2) the block faulting, or thick-skinned, style of the Laramide [Berg, 1962; Prucha et al., 1965; Smithson et al., 1979] and Pampeanas [Jordan et al., 1983] ranges. In the Andes, while the thin-skinned deformation occurs over both nearly horizontal and shallow dipping (≈ 30°) subducting slabs, the thick-skinned deformation is limited to regions where the slabs are nearly horizontal. In the western United States the development of the Laramide basement faults was accompanied by an eastward migration of the volcanic arc, and this has led to the popular view that the slab was very shallowly dipping during the episode of Laramide deformation.

The style of deformation in the Bali Basin appears to be intermediate between that of the thin-skinned style east of the Andes and Rockies

and the basement block faulting of the Laramide or the Pampeanas. While the earthquakes examined in this report certainly occur within basement, and not along a decollement at the base of the sedimentary sequence, they are also of fairly low angle, and the associated basement faults do not seem to extend into the sedimentary layer. The sediments respond to basement shortening by folding and are probably decoupled from basement along an aseismic shallow dipping plane that steepens into basement and becomes seismic only beneath the southern edge of the Bali Basin. The Madura-Kangean, Meratus, and Pulau Laut ridges are basement uplifts that sit in the same tectonic position as the Laramide and Pampeanas basement uplifts, and are probably the roots of anticlines formed by compression [Ben-Avraham and Emery, 1973].

The Java-Bali section of the Sunda arc is a likely analog for the initial stages of thrusting on the east side of the Andes [Jordan et al., 1983]. Suarez et al. [1983] propose an evolutionary scenario for the Andes that begins with the Brazilian Shield thrusting westward beneath the volcanic chain, forming a small foreland basin and uplifting the mountain belt. As the thrusting and uplift proceed, it becomes easier to form a new thrust zone within the shield to the east than to continue uplifting the mountains. Suarez et al. [1983] envision that the lateral growth of the Andes proceeds by successive eastward jumps in the locus of thrusting and uplift. Such outward (eastward) migration of foreland thrusting may have also occurred in western North America [e.g., Armstrong and Oriel, 1965], though this view is not held by all [Mountjoy, 1966].

We suggest a scenario for the growth of the arc in the Java-Bali region of the Sunda arc that is similar to that proposed for the Andes by Suarez et al. [1983] but in its infancy. The Sunda arc example also suggests that discrete jumps in the locus of faulting proceed along strike as well as outward from the mountain belt. The evolutionary sequence along strike is exemplified here by the spatial and temporal development of the Java, Bali, and Flores basins.

The greater widths of Java and Sumatra than those of the islands to the east are not due to voluminous magmatic activity but rather because of the exposure of the foreland basins. The Java Basin in the Tertiary was a shallow marine basin bordered on the north by the subaerial Sunda Shelf and to the south by an active volcanic arc [Weeda, 1958]. (A similar basin formed in Sumatra [Katili, 1974], but we limit our discussion to the Java Basin.) Prior to the development of the Java Basin, the Sunda Shelf probably extended to the present south coast of Java, and accordingly, the Java Basin formed as a downwarp in the Sunda Shelf. The 6-km-thick sedimentary sequence in the Java Basin reveals a marine transgression in the Oligocene, bathyal marine conditions in the Miocene, and land conditions by Pliocene [Hamilton, 1979; Weeda, 1958]. Folding in the west Java Basin began in the Miocene when bathyal conditions prevailed [Hamilton, 1979] and the intensity of folding decreased toward the Madura Basin to the east and toward the volcanic arc to the south [Weeda, 1958]. The end of sedimentation in the Java Basin is marked by emergence and a major orogenic phase in middle to late Pleistocene [Soetantri et al., 1973]. Today in the Madura and Java basins, the younger sediments are less deformed than the older, but even upper Quaternary sediments are involved in the compressional deformation [Hamilton, 1979; Weeda, 1958]. The total amount and present rate of shortening in the Java Basin are unknown, but the lack of earthquakes or gravity anomalies suggests that they are small, despite the evidence for continued deformation [Weeda, 1958].

Activity began in the Bali Basin as it waned in the Java Basin, and we are probably witnessing a similar progression under way in the Bali Basin. However, we do not intend to infer a causal relationship between the onset of deformation in one basin and its demise in the other. The high variability in the character of back arc thrusting now along the Sunda Arc indicates that the thrusting is strongly dependent on conditions in the fore arc as well as the back arc [Silver et al., 1983]; hence the eastward migration of activity in the back arc from Java to Bali may reflect some fore arc process (such as migration of the Roo Rise), as easily as a back arc process (for instance, the resistance of the buoyant Sunda Shelf to thrusting beneath the volcanic arc). The point is that to future geologists, the Java and Bali basins may appear as a linear zone of deformation but will be characterized by greatly different histories. Also structurally on line with the Bali and Java basins will be the suture along which the Flores Basin closed. The Flores Basin, while undergoing closure concurrently with the Bali Basin, is morphologically distinct from the Bali Basin in that it is floored by oceanic crust and is much deeper. With the exceptions of subtle sedimentological facies differences and the possibility that its suture will be marked by ophiolites, the structures resulting from closure of the Flores Basin may be indistinguishable from those in the Bali Basin. The picture will be complicated further if new fold-and-thrust belts develop outboard (north) of the old, as in the scenario of Suarez et al. [1983].

Summary

The focal depths and fault plane solutions for eight earthquakes from the Bali Basin have been determined by inversion of long-period P and SH waves and short-period P waves. The results indicate that thrusting occurs beneath the southern margin of the Bali Basin at depths that range from 10 to 18 km and on planes that dip to the south at angles between 13° and 35°. The events had seismic moments that range from 4×10^{17} to 7×10^{18} Nm, and several were quite destructive. Summation of seismic moments suggests a minimum closure rate of 4 ±2 mm/a over the past 25 years.

Characteristics of the waveforms and the earthquake locations with respect to crustal models constrained by gravity and seismic data suggest that the earthquakes occurred primarily within the crystalline basement, beneath the sedimentary layer. The south dipping nodal planes that we infer to be the fault planes dip too steeply to be due to thrusting on a zone of decollement between the basement and the sediment

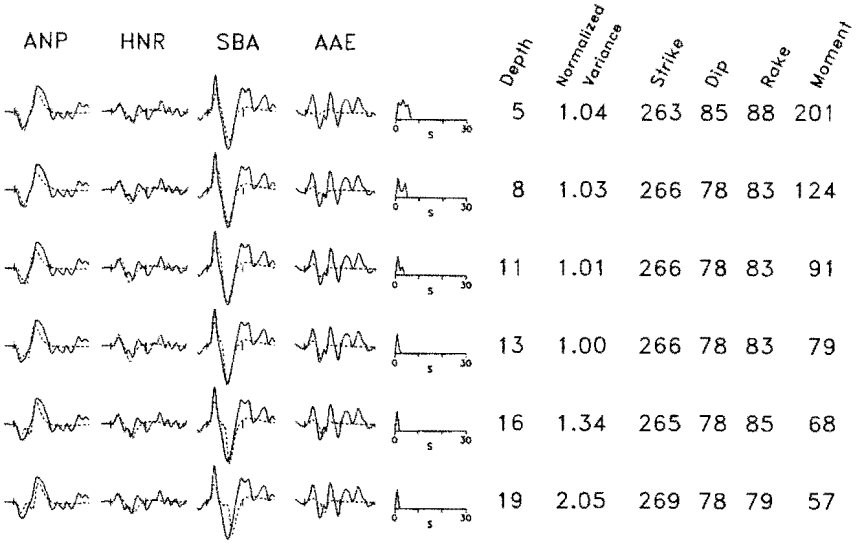

Fig. 11a. Comparison of observed (solid lines) and calculated (dashed lines) P wave seismograms of event 2 for a range of depths. The depth is held fixed, while the remaining parameters (strike, dip, rake, moment, and the source time function) are determined by inversion. The variance is normalized by the variance of the best fitting solution. Seismic moment is in units of 10^{16} Nm.

layer but also too shallowly to be analogous to the steep faults along which thick basement blocks are uplifted, such as during the Laramide faulting of western North America or in the Pampeanas Ranges of the Andes. These earthquakes probably reveal some intermediate activity, such as basement shortening south of the foreland fold-and-thrust belt that is represented by the central part of the Bali Basin.

The similarity of the slip vectors of the eight earthquakes to the convergence direction between the Asian and Indian Ocean plates suggests that the thrusting in the back arc region is related to plate convergence. Collision or strongly coupled subduction is indicated. However, because the arc is extensively cut by strike-slip faults, it is probably quite weak, and the thrusting here is not easily relatable to the collision with the Australian continent that occurs several hundred kilometers to the east. Moreover, the Mesozoic age of the subducting lithosphere, the morphology of the fore arc south of Bali, the lack of thrust events beneath the fore arc, and a preponderance of large, shallow normal faulting events at the Java Trench suggest that the upper and lower plates are weakly coupled. The only likely scenario involving a collision is interaction with the Roo Rise, a broad feature with approximately 1 km of relief that rises above the Indian Ocean floor and intersects the Java Trench south of Java and Bali.

Finally, we propose a scenario for the development of the Bali, Java, and Flores basins that has implications for the development of continental fold-and-thrust belts and for the growth of continental arcs such as the Andes and western North America. The island of Java has nearly doubled in width during the Tertiary by the addition of a wide and deep sedimentary basin to its back side. This basin likely formed in the Sunda Shelf and was filled by sediments from both the magmatic arc to the south and from the Sunda Shelf to the north. The same process occurs now in the Bali Basin. Folding and thrusting within the Java Basin continue to the present but have declined in intensity, and the Java Basin is now exposed. The Bali Basin formed east of the Java Basin and is now in the process of being closed by thrusting. To the east of the Bali Basin, the Flores Basin, of oceanic origin, is actively closing by thrusting at its southern margin. This example suggests that individual thrust episodes may migrate along strike as well as outward from mountain belts.

Appendix

The formal uncertainties in the earthquake source parameters determined by the inversion procedure underestimate the true uncertainties. Here, we briefly assess the realistic uncertainties, examine the possible trade-offs between parameters, and present our strategies for deciding on the best solution. The procedure followed is to fix the parameter being examined at values that bracket the best fitting value and solve for the remaining parameters. In the figures that follow, only selected seismograms are shown, but all calculations were done with all the available seismograms (Figure 6).

Focal Depths

For the range of depths, source durations, and mechanisms presented in this paper, events 2, 6, and 8 are probably representative and are used to examine depth uncertainties. For event 2 (Figure 11a), the trade-off between the depth, source duration, and dip angle results in very little increase in variance between 5- and 13-km depth. At depths greater than 13 km the reflected phases are too late, resulting in phase mismatch and large variance. We feel that a diagnostic seismogram is at AAE, for which the shallower solutions

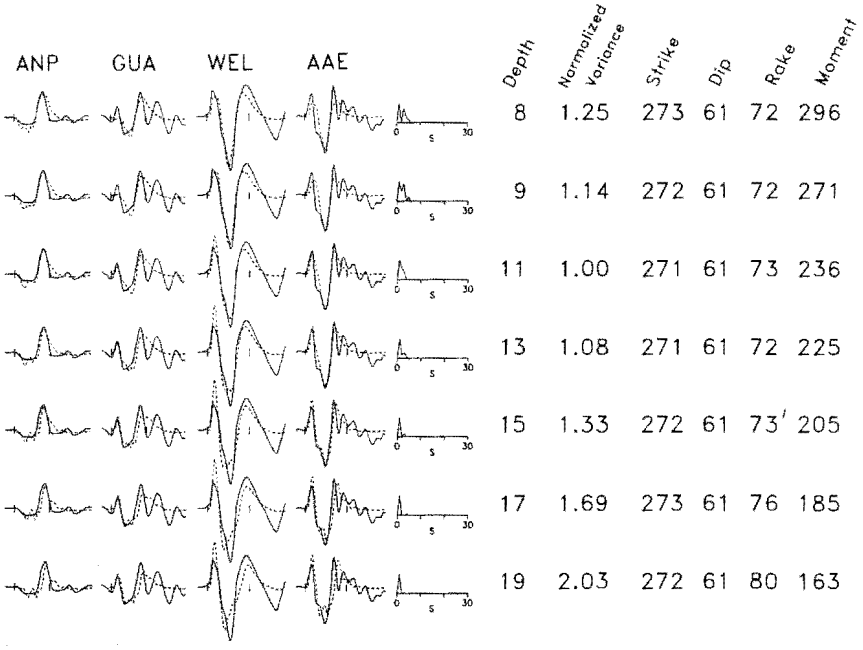

Fig. 11b. Comparison of observed and calculated P wave seismograms of event 6 for a range of depths. Format as in Figure 11a.

give a poor fit to the P wave because of the increase in the dip angle. From this, we infer that event 2 is no deeper than 16 km and no shallower than 8 km. Although the P wave seismogram at AAE was not available for event 1, we suggest that the uncertainty in its depth is also ±5 km, based on the similarity of the seismograms to those of event 2, and the proximity in time and space of the two events.

Event 6 (Figure 11b) shows less trade-off between the depth and other parameters. Although the source duration increases, the dip angle is more stable than for event 2 and the variance increases with decreasing depth. This stability in the dip angle is due to the increase in the relative strength and number of P wave seismograms with P and pP phases of opposite polarity (such as AAE for event 2). For the shallower

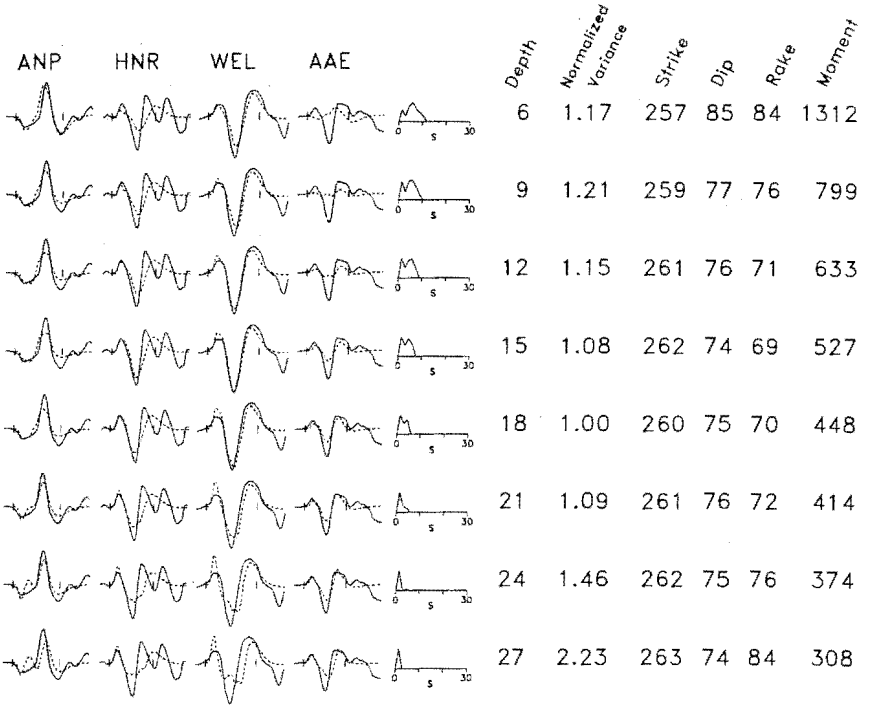

Fig. 11c. Comparison of observed and calculated P wave seismograms of event 8 for a range of depths. Format as in Figure 11a.

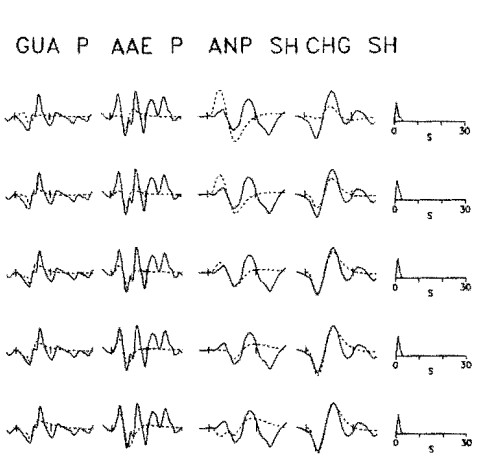

Fig. 11d. Comparison of observed and calculated P and SH wave seismograms of event 2 for a range of strike angles. Format as in Figure 11a.

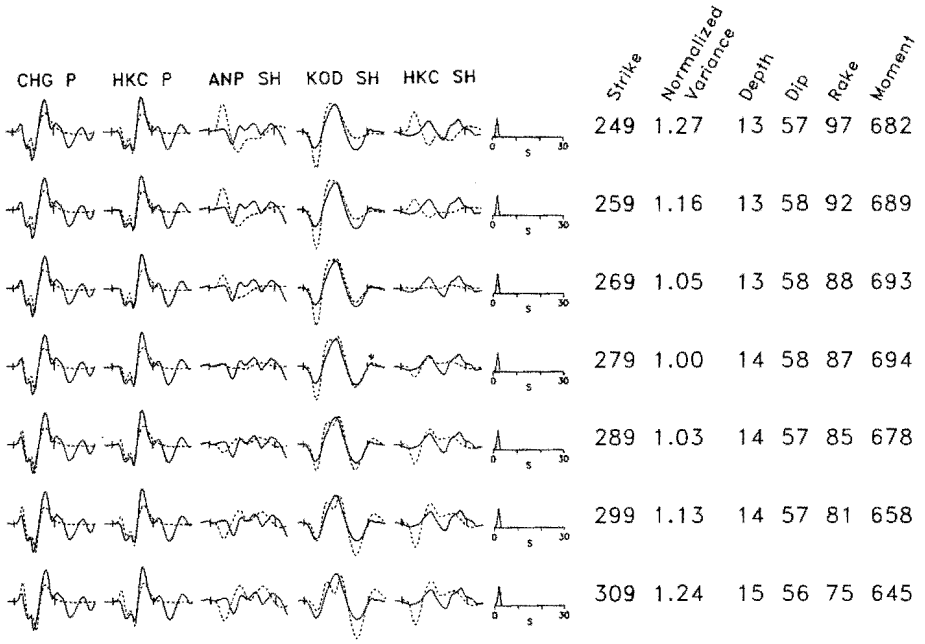

Fig. 11e. Comparison of observed and calculated P and SH wave seismograms of event 3 for a range of strike angles. Format as in Figure 11a.

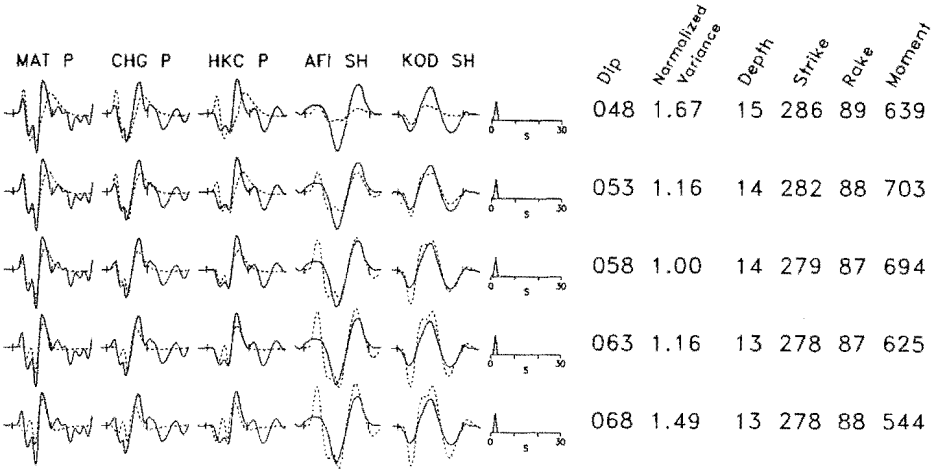

Fig. 11f. Comparison of observed and calculated P and SH wave seismograms of event 3 for a range of dip angles. Format as in Figure 11a.

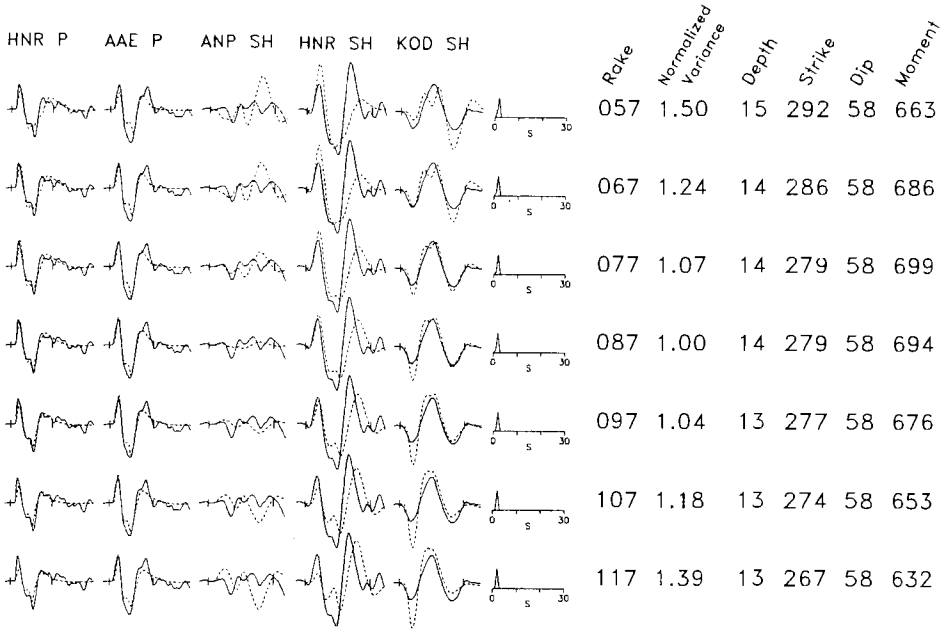

Fig. 11g. Comparison of observed and calculated P and SH wave seismograms of event 3 for a range of rake angles. Format as in Figure 11a.

assumed sources, the initial cycle of the calculated seismogram for GUA becomes small because of the destructive interference between P and pP. The estimated uncertainty in depth of ±4 km for this event probably also applies to events 3, 4, 5, and 7, because of the similarity in their mechanisms and station distributions.

Event 8 (Figure 11c) is similar in depth and orientation to event 1 but has a longer source duration. As for event 2, there is trade-off between depth and source duration but over a greater range of depths; from 12 to 24 km. Above 9 km the variance decreases because of the change in dip but again this produces an unacceptable fit at AAE.

The uncertainty in source depths and the variations in seismic moment with depth introduce an uncertainty of approximately 50% in the estimated seismic moments (Figures 11a, 11b, and 11c). An additional systematic bias in the depth is caused by the uncertainty in the velocity used to calculate seismograms. If the average velocities in the earth above the source range from 5.5 to 7.5 km/s, the bias in depth will be about ±20% of the calculated depth.

Orientation

The uncertainties in strike, dip, and rake angles are given for the north dipping nodal planes. For event 2 (and by similarity, for events 1 and 8), the uncertainty in strike is between 10° and 20° (Figure 11d). For this mechanism the near-nodal P and SH waves are most sensitive to strike, but there is a trade-off with the rake angle. The uncertainty in strike for event 3 (and events 4-7) is greater (±20-30°; Figure 11e) than that for event 2 despite the decrease in trade-off with the rake angle.

The dip angle of the north dipping nodal plane is constrained to within ±5° (Figure 11f). The most obvious constraints are the polarities of the P waves, but the SH wave amplitudes are also sensitive to the dip angle. Because the dip angle is determined largely by seismograms at the northern stations, it will vary directly with the takeoff angles for rays to these stations. For a range in source velocities from 5.5 to 7.5 km/s, the takeoff angles and thus dip angles will vary by ±5° for a dip angle of 60° and by ±2° for a dip angle of 75°.

The uncertainty in the rake angle for event 3 is approximately 20° (Figure 11g) and is probably similar for the other events. The rake angle is largely constrained by the SH waves but trades off strongly with the strike angle. Note that a difference in the rake angle of 20° on the north dipping auxiliary plane corresponds to differences in the south dipping (fault) plane of approximately 30° in strike and less than 5° in dip (compare in Figure 6 events 3 and 5, whose rake angles differ by 18°).

Throughout the tests of the orientation parameters, the depth (±1 km), source duration (±1 s), and seismic moment (±10%) remain stable.

Acknowledgments. We thank P. Molnar for helpful discussions, E. A. Silver and R. K. Cardwell for reviews, and Z. Ben-Avraham for permission to reproduce the bottom half of Figure 4. This work was funded by NSF grant EAR-8319250 and in part by the Air Force Geophysics Scholar Program.

References

Aki, K., and P.G. Richards, Quantitative Seismology, Theory and Methods, 557 pp., W.H. Freeman, San Francisco, Calif., 1980.

Armstrong, R.L., Sevier orogenic belt in Nevada and Utah, Bull. Geol. Soc. Am., 79, 429-458, 1968.

Armstrong, R.L., and S.S. Oriel, Tectonic development of Idaho-Wyoming thrust belt, Bull. Am. Assoc. Pet. Geol., 49, 1847-1866, 1965.

Bally, A.W., P.L. Gordy, and G.A. Stewart,

Structure, seismic data, and orogenic evolution of the southern Canadian Rocky Mountains, Can. Pet. Geol. Bull., 14, 337-381, 1966.

Ben-Avraham, Z.; Structural framework of the Sunda Shelf and vicinity, Ph.D. thesis, 269 pp., Mass. Inst. of Technol., Cambridge, and Woods Hole Oceanogr. Inst., Mass., 1973.

Ben-Avraham, Z., and K.O. Emery, Structural framework of Sunda Shelf, Bull. Am. Assoc. Pet. Geol., 57, 2323-2366, 1973.

Berg, R.R., Mountain flank thrusting in Rocky Mountain foreland, Wyoming and Colorado, Bull. Am. Assoc. Pet. Geol., 46, 2029-2032, 1962.

Boatwright, J., A spectral theory for circular seismic sources; simple estimates of source dimensions, dynamic stress drop, and radiated seismic energy, Bull. Seismol. Soc. Am., 70, 1-27, 1980.

Bowin, C.O., W. Warsi, and J. Milligan, Free-air gravity anomaly atlas of the world, Geol. Soc. Am. Map Chart Ser., MC-46, 1982.

Brune, J.N., Seismic moment, seismicity, and rate of slip along major fault zones, J. Geophys. Res., 73, 777-784, 1968.

Caldwell, W.F., W.F. Haxby, D.E. Karig, and D.L. Turcotte, On the applicability of a universal elastic trench profile, Earth Planet. Sci. Lett., 31, 239, 1976.

Cardwell, R.K., and B.L. Isacks, Geometry of the subducted lithosphere beneath the Banda Sea in eastern Indonesia from seismicity and fault plane solutions, J. Geophys. Res., 87, 2825-2838, 1978.

Cardwell, R.K., E.S. Kappel, M.S. Lawrence, and B.L. Isacks, Plate convergence along the Indonesian arc (abstract), Eos Trans. AGU, 62, 404, 1981.

Curray, J.R., G.G. Shor, R.W. Raitt, and M. Henry, Seismic refraction and reflection studies of crustal structure of the eastern Sunda and western Banda arcs, J. Geophys. Res., 82, 2479, 1977.

Effendi, I., T. Priantono, S. Tjokrosapoetro, and K. Budiono, Overview of disastrous tectonic earthquakes in the period between April 1979 - April 1980, Bull. Geol. Res. Dev. Cent. Indones., 4, 18-20, 1981.

Fitch, T.J., Earthquake mechanisms and island arc tectonics in the Indonesian-Philippine region, Bull. Seismol. Soc. Am., 60, 565-591, 1970.

Fitch, T.J., R.G. North, and M.W. Shields, Focal depths and moment tensor representations of shallow earthquakes associated with the great Sumba earthquake, J. Geophys. Res., 86, 9357-9374, 1981.

Futterman, W.I., Dispersive body waves, J. Geophys. Res., 67, 5279-5291, 1962.

Ganse, R.A., and J.B. Nelson, Catalog of significant earthquakes 2000 B.C. - 1979, Including quantitative casualties and damage, 154 pp., World Data Cent. A for Solid Earth Geophys., Boulder, Colo., 1981.

Grow, J.A., and C.O. Bowin, Evidence for high-density crust and mantle beneath the Chile trench due to the descending lithosphere, J. Geophys. Res., 80, 1449-1458, 1975.

Hamilton, W., Tectonics of the Indonesian region, U.S. Geol. Surv. Prof. Pap. 1078, 345 pp.,1979.

Herrin, E., 1968 seismological tables for P phases, Bull. Seismol. Soc. Am., 58, 1193-1352, 1968.

Jordan, T.E., B.L. Isacks, R.W. Allmendinger, J.A. Brewer, V.A. Ramos, and C.J. Ando, Andean tectonics related to geometry of subducted Nazca plate, Bull. Geol. Soc. Am., 94, 341-361, 1983.

Kappel, E.S., Plate convergence in the Sunda and Banda arcs, B.A. thesis, 40 pp., Cornell Univ., Ithaca, N.Y., 1980.

Katili, J.A., Sumatra, in Mesozoic-Cenozoic Orogenic Belts, Data for Orogenic Studies, Geol. Soc. London Spec. Publ., vol. 4, edited by A.M. Spencer, pp. 317-331, Scottish Academic Press, 1974.

Kelleher, J., and W. McCann, Buoyant zones, great earthquakes, and unstable boundaries of subduction, J. Geophys. Res., 81, 4885-4896, 1976.

Larson, R.L., Late Jurassic sea-floor spreading in the eastern Indian Ocean, Geology, 3, 69-71, 1975.

McCaffrey, R., and J. Nabelek, The geometry of back arc thrusting along the eastern Sunda arc, Indonesia: Constraints from earthquake and gravity data, J. Geophys. Res., 89, 6171-6179, 1984.

McCaffrey, R., and J. Nabelek, Seismological evidence for shallow thrusting north of the Timor trough, Geophys. J. R. Astron. Soc., 85, 365-381, 1986.

McCaffrey, R., P. Molnar, S. Roecker, and Y. Joyodiwiryo, Microearthquake seismicity and fault plane solutions related to arc-continent collision in the eastern Sunda arc, Indonesia, J. Geophys. Res., 90, 4511-4528, 1985.

Minster, J.B., and T.H. Jordan, Present-day plate motions, J. Geophys. Res., 83, 5331-5354, 1978.

Molnar, P., Gravity anomalies and the origin of the Puerto Rico trench, Geophys. J. R. Astron. Soc., 51, 701-708, 1977.

Mountjoy, E.W., Time of thrusting in Idaho-Wyoming thrust belt -- Discussion, Bull. Am. Assoc. Pet. Geol., 50, 2612-2614, 1966.

Nabelek, J., Determination of earthquake source parameters from inversion of body waves, Ph.D. thesis, Mass. Inst. of Technol., Cambridge, 1984.

Nabelek, J., Geometry and mechanism of faulting of the 1980 El Asnam, Algeria, earthquake from inversion of teleseismic body waves and comparison with field observations, J. Geophys. Res., 90, 12713-12728, 1985.

Price, R.A., The Cordilleran foreland thrust and fold belt in the southern Canadian Rocky Mountains, in Thrust and Nappe Tectonics, Geol. Soc. London Spec. Publ., vol. 9, edited by K.R. McClay and N.J. Price, pp. 427-448, Blackwell Scientific, London, 1981.

Price, R.A., and E.W. Mountjoy, Geologic structure of the Canadian Rocky Mountains between Bow and Athabasca rivers -- A progress report, Geol. Assoc. Can., Spec. Pap., 6, 7-25, 1970.

Prucha, J.J., J.A. Graham, and R.P. Nickelson, Basement controlled deformation in Wyoming province of Rocky Mountain foreland, Bull. Am. Assoc. Pet. Geol., 49, 966-992, 1965.

Raitt, R.W., Marine seismic refraction studies of the Indonesian island arc (abstract), Eos Trans. AGU, 48, 217, 1967.

Ruff, L., and H. Kanamori, Seismicity and the subduction process, Phys. Earth Planet. Inter., 23, 240-252, 1980.

Silver, E.A., D.R. Reed, R. McCaffrey, and Y.S. Joyodiwiryo, Backarc thrusting in the eastern Sunda arc, Indonesia: A consequence of arc-continent collision, J. Geophys. Res., 88, 7429-7448, 1983.

Silver, E.A., N.A. Breen, H. Prasetyo, and D. Hussong, Multibeam study of the Flores backarc thrust belt, Indonesia, J. Geophys. Res., 91, 3489-3500, 1986.

Smithson, S.B., J.A. Brewer, S. Kaufman, J.E. Oliver, and C.A. Hurich, Structure of the Laramide Wind River uplift, Wyoming, from COCORP deep reflection data and from gravity data, J. Geophys. Res., 84, 5955-5972, 1979.

Soentantri, B., L. Samuel, and G.A.S. Nayoan, The geology of the oilfields in northeast Java, Proc. Indones. Pet. Assoc., 149-175, Second Annual Convention, Jakarta,, 1973.

Suarez, G., P. Molnar, and C. Burchfiel, Seismicity, fault plane solutions, depth of faulting, and active tectonics of the Andes of Peru, Ecuador, and southern Colombia, J. Geophys. Res., 88, 10,403-10,428, 1983.

Usna, I., S. Tjokrosapoetro, and S. Wiryosujono, Geological interpretation of a seismic reflection profile across the Banda Sea between Wetar and Buru islands, Bull. Geol. Res. Dev. Cent. Indones., 1, 7, 1979.

Uyeda, S., and H. Kanamori, Back arc opening and the mode of subduction, J. Geophys. Res., 84, 1049-1061, 1979.

van Bemmelen, R.W., The Geology of Indonesia, vol. 1A, 732 pp., Government Printing Office, The Hague, 1949.

Walcott, R.I., Flexural rigidity, thickness, and viscosity of the lithosphere, J. Geophys. Res., 75, 3941-3954, 1970.

Watts, A.B., and M. Talwani, Gravity anomalies seaward of deep-sea trenches and their tectonic implications, Geophys. J. R. Astron. Soc., 36, 57-90, 1974.

Watts, A.B., and M. Talwani, Gravity effect of downgoing lithospheric slabs beneath island arcs, Bull. Geol. Soc. Am., 86, 1-4, 1975.

Weeda, J., Oil basin of east Java, in Habitat of Oil, Am. Assoc. Pet. Geol., Spec. Publ., vol. 5802, edited by L.G. Weeks, pp. 1359-1364, 1958.

Woollard, G.P., The new gravity system--changes in international gravity base values and anomaly values, Geophysics, 44, 1352-1366, 1979.

R. McCaffrey, Department of Earth, Atmospheric and Planetary Sciences, Massachusetts Institute of Technology, Cambridge, MA 02139.

J. Nabelek, Lamont-Doherty Geological Observatory, Palisades, NY 10964.

(Received May 27, 1986;
revised August 25, 1986;
accepted August 27, 1986.)